IROS Workshop on Visual Control of Mobile Robots (ViCoMoR)
September 26, 2011, San Francisco, California, USA

One Homography to Control Multiple Robots

M. Aranda[1], G. López-Nicolás[1], Y. Mezouar[2] and C. Sagüés[1]

***Abstract*— This paper presents a visual control method to be used on a set of mobile robots. We consider a framework where the robots have nonholonomic constraints, move in a plane and are observed by a calibrated flying camera, which provides the only sensory information used for the control. The objective of the control task is to drive the group of robots to a desired configuration. This configuration is simply defined by an image, avoiding the need for additional information. The task is carried out through an image-based control scheme using the homography induced by the multi-robot system. Collision avoidance between the robots is also performed, using a simple image-based method. The performance of the proposal is illustrated through simulations.**

I. INTRODUCTION

Multi-robot systems are an important research area in current robotics, due to their suitability to perform certain tasks (such as exploration, surveillance, security or rescue operations) that are difficult for one single robot. In particular, a number of research works in this field focus on the problem of reaching and maintaining a robot team in a particular configuration [1] [2] [3].

Vision sensors have been extensively used for robot localization, navigation and control. Visual control is a wide field of research that has attracted the attention of many researchers [4]. In multi-robot systems, it is common to have a setup where each robot is equipped with a local perception system, and they share their information to accomplish the global task. This is the case, for example, in the localization method for multiple mobile robots presented in [5]. Another related work is [2], where groups of mobile robots are controlled to visually maintain formations, including the situation where communication between the robots is not available. The vision-based formation control with feedback-linearization proposed in [1] tackles the issue of switching between decentralized and centralized cooperative control.

Centralized multi-robot control approaches provide several advantages: they allow simple and cheap robots, and release their local resources by transferring expensive computations to an external computer. A centralized architecture is considered for the leader-follower control proposed in [3], where the perception system consists of a fixed camera on the ceiling. In general, vision-based tasks become more robust when multiple view geometry constraints are imposed [6]. Particularly, the homography is a well-known geometric model across two views induced by a plane of the scene, and it has been used extensively in visual control [7], [8], [9].

In this paper, we consider a framework where the multiple robots are assumed to have nonholonomic motion constraints and move in a planar surface. The goal of the proposed control scheme is to drive the multiple robots to a desired configuration defined by an image previously taken of that configuration. The visual information is acquired by a flying camera undergoing an arbitrary planar motion and looking downward at the robots. The camera moves in such a way that its translation is parallel to the motion plane of the robots and its rotation is parallel to the plane normal.

We propose a homography-based control approach that takes advantage of the planar motion constraint to parameterize the homography. With this particular parametrization, the approach can be used in a set of two or more robots. The image features we employ to compute the homography are the projections of the multiple robots on the image plane. Then, the computed homography gives information about the configuration of the set of robots. In particular, from the homography we can determine if the configuration of the robots is rigid, i.e. they maintain the desired configuration defined by the target image, or nonrigid, meaning that the robots are in a different configuration. We propose an image-based control law where a desired homography is defined as a reference for the control in order to drive the robots to the desired configuration. The use of the homography for multi-robot formation makes our approach different from other image-based techniques. In particular, the interaction is expressed and handled through this homography.

It is always necessary to perform collision avoidance when controlling multiple mobile robots. Being a key element of robotic navigation, obstacle avoidance has been extensively studied for many years. Classical solutions to the problem include the potential field methods [10]. These methods have some well-known shortcomings [11], which has prompted the appearance of many modifications and improvements on them [12], [13]. Potential-like methods continue to be widely used for obstacle avoidance, mainly due to their simplicity. Collision avoidance in multiple-robot scenarios has to deal with both inter-agent and external collisions. Simple, decentralized approaches are usually preferred. In our case, we use a potential-like collision avoidance method based on gyroscopic forces, similar to the approaches employed in [14], [15]. Our method is image-based, simple and fast to compute, well suited to nonholonomic vehicles, and can

[1] Instituto de Investigación en Ingeniería de Aragón. Universidad de Zaragoza, Spain. {marandac, gonlopez, csagues}@unizar.es

[2] LASMEA - Université Blaise Pascal, Aubiere 63177, France. youcef.mezouar@lasmea.univ-bpclermont.fr

This research was supported by grant I09200 from Gyeonggi Technology Development Program funded by Gyeonggi Province, by project DPI2009-08126, the ANR R-discover project, grant AP2009-3430 Ministerio de Educación and the I3A Fellowship Program.

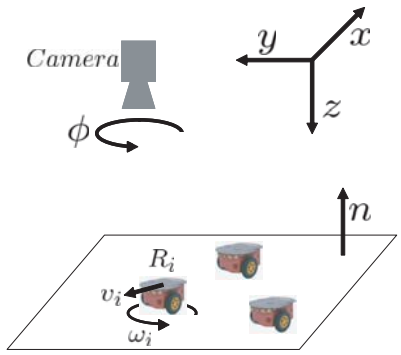

Fig. 1. Coordinate system: The motion of the camera occurs in the $x-y$ plane of the global reference and the robots undergo planar motion parallel to the $x-y$ plane. The rotation of the camera is also parallel to the plane normal $\mathbf{n}$.

be implemented as a decoupled term added directly to the control inputs.

This paper extends the work presented in [16]. Here, we propose a different control law which carries out the multi-robot configuration control task in one single step. With this scheme, only the positions of the robots in the configuration are controlled, while their final orientation is not regulated. This is suitable for cases where, for instance, the robots have omnidirectional capabilities, and the final orientation is irrelevant. The other main difference with respect to the aforementioned previous work is that in this paper we incorporate a collision avoidance mechanism, which is a necessary element in any multi-robot control implementation.

The paper is organized as follows. Section II presents the parametrization of the homography and the definition of the desired homography for reaching the multi-robot goal configuration. The control law for the multi-robot system and the collision avoidance method employed are presented in section III. In Section IV the performance of the proposal is illustrated through simulations. Finally, the conclusions of the paper are given in Section V.

II. Homography-Based Scheme

The setup of the multi-robot system and the flying camera is illustrated in Fig. 1, where the global fixed Left-handed coordinate system is depicted. In the following, we parameterize the homography in this framework and describe the method to compute linearly the homography. Then, we propose a procedure to define the desired homography that corresponds to the desired configuration of the multi-robot system.

A. Homography Parametrization

Two perspective images can be geometrically linked through a plane by a homography $\mathbf{H} \in \mathbb{R}^{3\times3}$. This projective transformation $\mathbf{H}$ relates points of the plane projected in both images. Pairs of corresponding points $(\mathbf{p}, \mathbf{p}')$ are then related up to scale by $\mathbf{p}' = \mathbf{H}\,\mathbf{p}$. The calibrated homography can be related to camera motion and plane parameters as follows

$$\mathbf{H} = \mathbf{R} + \mathbf{T}\,\mathbf{n}^T/d\,, \tag{1}$$

where $\mathbf{R}$ and $\mathbf{T}$ are the relative rotation and translation of the camera, $\mathbf{n}$ is the unit normal of the plane with respect to the reference frame and d is the distance along $\mathbf{n}$ between the plane and the reference position. In the framework considered, the position of the camera $(x, y, z)^T$ is constrained to the plane $x-y$ (i.e. $z=0$) and rotation ϕ about the z-axis. This constraint yields

$$\mathbf{R} = \begin{bmatrix} \cos\phi & \sin\phi & 0 \\ -\sin\phi & \cos\phi & 0 \\ 0 & 0 & 1 \end{bmatrix}\,,\quad \mathbf{T} = \begin{pmatrix} t_x \\ t_y \\ t_z \end{pmatrix}\,, \tag{2}$$

with $\mathbf{T} = -\mathbf{R}(x, y, 0)^T$.

In our framework, the mobile robots move in a planar surface that generates the homography. Besides, the camera undergoes planar motion: the translation is parallel to the plane and the rotation is parallel to the plane normal, i.e. the z-axis, and $\mathbf{n} = (0, 0, -1)^T$. Notice that the distance d is the height of the camera with respect the motion plane of the robots. Therefore, the homography matrix is given by

$$\begin{aligned} \mathbf{H} &= \begin{bmatrix} h_{11} & h_{12} & h_{13} \\ h_{21} & h_{22} & h_{23} \\ 0 & 0 & 1 \end{bmatrix} \\ &= \begin{bmatrix} \cos\phi & \sin\phi & -t_x/d \\ -\sin\phi & \cos\phi & -t_y/d \\ 0 & 0 & 1 \end{bmatrix}\,. \end{aligned} \tag{3}$$

B. Homography Computation

The homography across two views can be computed from a minimal set of four point correspondences solving a linear system [17]. In our framework, the points considered consist of the projection of the robots on the image plane, and they are denoted in homogeneous coordinates by $\mathbf{p} = (p_x, p_y, 1)$. A point correspondence $(\mathbf{p}, \mathbf{p}')$ is related up to scale by the homography as $\mathbf{p}' = \mathbf{H}\mathbf{p}$, which can be expressed in terms of the vector cross product as $\mathbf{p}' \times \mathbf{H}\mathbf{p} = \mathbf{0}$ [17]. From this expression two linearly independent equations in the entries of $\mathbf{H}$ (3) are obtained

$$\begin{bmatrix} p_x & p_y & 1 & 0 & -p'_x \\ p_y & -p_x & 0 & 1 & -p'_y \end{bmatrix} \begin{pmatrix} h_{11} \\ h_{12} \\ h_{13} \\ h_{23} \\ h_{33} \end{pmatrix} = 0\,. \tag{4}$$

Each point correspondence gives two independent equations. Given that $\mathbf{H}$ is defined by seven unknown entries, and using the homography constraints $h_{11} = h_{22}$ and $h_{21} = -h_{12}$, a set of two point correspondences allows to determine the homography up to a scale factor by solving a linear system. Given that h_{33} is never zero because of the particular form (3), the scale of the homography can always be normalized and fixed by this entry.

C. The Target Homography

Each pair of robots induce a homography across two images, the current image and the image of the desired configuration. Given a set of N robots, the number of homographies defined by the different pair of robots is

$N(N-1)/2$. If all of these homographies are equal, the relative motion of the robots is rigid. Otherwise, if any of the homographies is different to the others, the relative motion of the set of robots is not rigid and they are not in the desired configuration. A desired homography computed using all robots needs to be defined in order to lead the robots to the desired configuration.

In the first case, the homography induced by the plane of the robots moving in the desired configuration is conjugate to a planar Euclidean transformation given by

$$\mathbf{H}_{rigid} = \begin{bmatrix} \cos\phi & \sin\phi & h_{13} \\ -\sin\phi & \cos\phi & h_{23} \\ 0 & 0 & 1 \end{bmatrix} . \quad (5)$$

Notice that the upper left hand 2×2 matrix is orthogonal. The Euclidean transformation produces a translation and rotation of the image, and lengths and angles are invariants by this transformation.

The angle of rotation is encapsulated in the eigenvalues of (5) given by $\{1, e^{i\phi}, e^{-i\phi}\}$. Then, from the general expression of the homography, it can be deduced that $\mathbf{n} = (0,0,-1)^T$ and relative motion up to scale $(x,y,0)^T$ analogue as the assumptions defined for the homography parametrization. In this case, the robots are in formation with all the homographies induced by pairs of robots equal to the homography computed from all the robots (5) .

In the second case, the motion of the robots is not rigid, and they are not in the desired configuration. Then, the computation of the homography gives a matrix of the form

$$\mathbf{H}_{nonrigid} = \begin{bmatrix} s\cos\phi & s\sin\phi & h_{13} \\ -s\sin\phi & s\cos\phi & h_{23} \\ 0 & 0 & 1 \end{bmatrix} , \quad (6)$$

where the upper left hand 2×2 matrix is no longer orthogonal. This previous matrix corresponds to a similarity transformation, i.e. translation, rotation and isotropic scaling represented by the scalar s. Angles and ratios of lengths are invariants by this transformation. The eigenvalues of this similarity are $\{1, s\,e^{i\phi}, s\,e^{-i\phi}\}$ and encapsulate the rotation angle. Comparison with the general expression of the homography leads again to $\mathbf{n} = (0,0,-1)^T$ but to a computed relative motion $(x, y, (s-1)d^2)^T$ up to scale, with $z \neq 0$. Therefore, the nonrigid motion of the robots induces a valid homography but not constrained to the assumed camera motion. We need to define a desired homography like $\mathbf{H}_{nonrigid}$, but being induced by a motion that keeps the camera motion constraints. This can be done normalizing (6) to make the upper left hand 2×2 matrix orthogonal and setting $h_{33} = 1$ to hold the planar motion constraint of the camera ($z = 0$). Alternatively, we can simply normalize the upper left hand 2×2 matrix and obtain the desired homography with

$$\mathbf{H}^d = \mathbf{H}_{nonrigid} \begin{bmatrix} 1/s & 0 & 0 \\ 0 & 1/s & 0 \\ 0 & 0 & 1 \end{bmatrix} , \quad (7)$$

where s is computed as the norm of the upper left hand 2×2 matrix of $\mathbf{H}_{nonrigid}$. Then, the goal is to control the robots in such a way that all the homographies are led to $\mathbf{H}^d$ to reach the desired configuration.

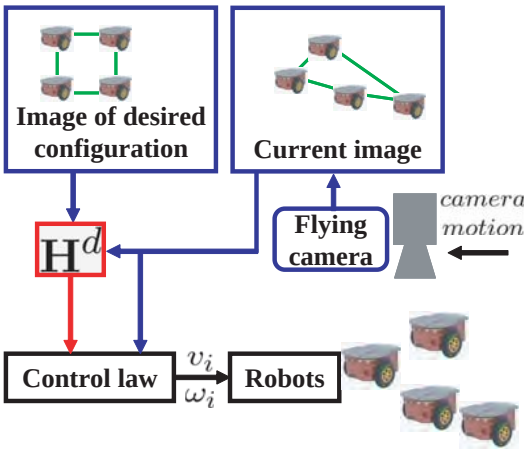

Fig. 2. Overview of the control loop. In each iteration of the control, the flying camera takes a current image of the robots, the desired homography $\mathbf{H}^d$ is obtained and used in the control law to compute the robot velocities necessary to reach the desired configuration of the multi-robot system.

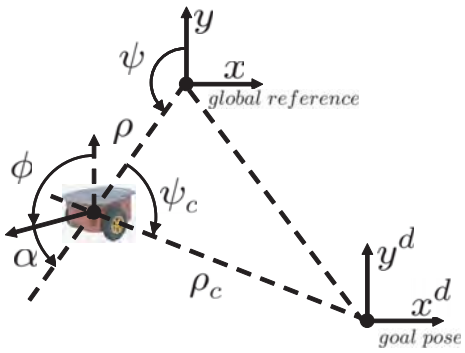

Fig. 3. Coordinate systems from a top view of the 3D scene. The robot position is given by $(x,y,\phi)^T$ or $(\rho,\alpha,\phi)^T$ in the global reference. The different parameters depicted are described along the text.

The $\mathbf{H}_{nonrigid}$ relates each point $\mathbf{p}$ of the current image with the corresponding point $\mathbf{p}'$ in the desired formation image with $\mathbf{p}' = \mathbf{H}_{nonrigid}\,\mathbf{p}$. The desired homography $\mathbf{H}^d$ is used now to define the goal location of the points in the image as $\mathbf{p}^d = (\mathbf{H}^d)^{-1}\,\mathbf{p}'$. Notice that the desired location of the robots in the image computed from the desired homography is not constant and varies along the time depending on the motion of the camera and the robots.

III. Visual Control Law

From the desired homography computed as explained in the previous section, we propose a control scheme to drive the robots to the desired configuration defined by an image of that configuration. An overview of the control loop is depicted in Fig. 2.

A. Robot Model and Coordinate Systems

Different coordinate systems defined in the 3D space are depicted in Fig. 3. The state of each robot is given by $(x,y,\phi)^T$, where ϕ is the orientation of the robot expressed

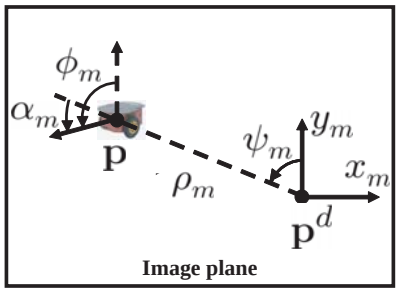

Fig. 4. Coordinate systems on the image plane for each robot. Subindex m denotes that the variable is defined on the image plane (the same variable without subindex m refers to the 3D space). Point $\mathbf{p}$ is the image projection of a robot and $\mathbf{p}^d$ its location to reach the desired configuration of the multi-robot system.

as the angle between the robot body y-axis and the world y-axis. Each robot has two velocity inputs, the linear velocity v and angular velocity ω, with v in the direction of the robot y-axis, and ω about the robot z-axis. The kinematics of each robot can be then expressed in general in polar or Cartesian coordinates in a fixed reference as

$$\begin{cases} \dot{\rho} = v\,\cos\alpha \\ \dot{\alpha} = \omega - \frac{v}{\rho}\sin\alpha \\ \dot{\phi} = \omega \end{cases} \text{, and } \begin{cases} \dot{x} = -v\,\sin\phi \\ \dot{y} = v\cos\phi \\ \dot{\phi} = \omega \end{cases} , \quad (8)$$

respectively, being

$$x = -\rho\sin\psi \quad \text{and} \quad y = \rho\cos\psi\ . \quad (9)$$

The alignment error α is defined as the angle between the robot body y-axis and the distance vector ρ,

$$\alpha = \phi - \psi\ . \quad (10)$$

We now introduce several variables, depicted in Fig. 4, to define the state of each robot on the image plane with (ρ_m, ψ_m, ϕ_m). The origin of the coordinate system for each robot $\mathbf{p}$ on the image plane is placed in the desired location $\mathbf{p}^d$, i.e. the robots are in the desired configuration when all of them are in the origin of their respective references ($\mathbf{p}^d$).

The variable ρ_m denotes the distance of the projection of a robot in the image $\mathbf{p}$ with respect to its desired position on the image $\mathbf{p}^d$, and so

$$\rho_m = \sqrt{(p_x - p_x^d)^2 + (p_y - p_y^d)^2}\ , \quad (11)$$

and also

$$\psi_m = atan2\left(-(p_x - p_x^d), (p_y - p_y^d)\right)\ , \quad (12)$$

where function $atan2$ returns the value of the arc tangent using the sign of the arguments to determine the quadrant. ϕ_m can be computed directly from the image of the robot with computer vision techniques or estimated with $\phi_m = atan2(-\Delta p_x, \Delta p_y)$, where Δp_x and Δp_y is the incremental motion of the robot in the image plane. The alignment error on the image α_m is also defined as $\alpha_m = \phi_m - \psi_m$.

B. Control Law

We define the control law in order to bring the robot team to the desired configuration. The control is carried out in one single step. It is assumed that the final orientation of the agents is not relevant. This would be the case, for example, in an application where a secondary task is performed by robots having omnidirectional capabilities. Having this assumption in mind, we define the controller as follows:

$$\begin{cases} v = -k_v\,\rho_m \\ \omega = -k_\omega\,(\alpha_m - \pi) \end{cases} , \quad (13)$$

where $k_v > 0$ and $k_\omega > 0$ are control gains.

This control law drives the robots to their target positions so that the team reaches the desired configuration. The image projection of the distance to the desired position ρ_m and the alignment error α_m are measured directly in the image plane.

C. Collision avoidance

We choose to perform the collision avoidance task with a method based on gyroscopic forces. These types of approaches [14], [15] have their origin in navigation function methods (NFM) [18], and present some interesting properties. First, they are simple and fast. In addition, they are suitable to be used directly on a nonholonomic vehicle as steering commands. Gyroscopic forces can be implemented simply as an additive term in the control law, decoupling the collision avoidance from the control task. Also, their application does not change the energy of the system, which is an interesting characteristic from the stability viewpoint. Lastly, they are known to be able to avoid certain trap situations that come about with collision avoidance methods based on navigation functions.

In order to avoid inter-agent collisions, we use the following repulsive potential function [10] between any two given robots in the team:

$$f_{ij}(r_{ij}) = \begin{cases} \frac{1}{2}\eta\left(\frac{1}{r_{ij}} - \frac{1}{r_0}\right)^2, & r_{ij} \le r_0 \\ 0, & r_{ij} > r_0. \end{cases} \quad (14)$$

This function has been widely used in obstacle avoidance contexts. It creates a repulsive force when the distance (r_{ij}) between two agents i and j is below a certain limit distance (r_0). In [14], [15], split-rejoin behaviors of the team of robots are desired, and therefore the potential functions employed are different from ours. Collision avoidance needs range information; however, due to the particular geometry of our framework, distances in the image plane are equivalent to distances between the robots, up to a constant scale factor. This allows us to implement the collision avoidance (i.e. compute (14)) using only visual information. The total repulsive potential acting on each robot is equal to the sum of the potentials due to all of the other robots in the group, i.e. $f_i = \sum_{j \neq i} f_{ij}(r_{ij})$.

We perform the collision avoidance as an additive angular velocity term. The linear velocity remains unchanged. The

added steering term for every robot i is proportional to the negative gradient of the potential function projected on the direction orthogonal to the orientation of the robot ($v_i^{\perp}$):

$$\omega_i^{ca} = -k_{ca} < v_i^{\perp}, \nabla_{r_i} f_i >, \qquad k_{ca} > 0. \tag{15}$$

The total angular velocity of the control method is:

$$\omega^{total} = \omega + \omega^{ca}, \tag{16}$$

where ω is given by (13).

IV. Experiments

In this section, we present several simulations in order to illustrate the performance of the control scheme. It is assumed that the projection of each robot in the images can be detected and identified in order to match it with its correspondence in the other images.

The first experiment considers a configuration consisting of four robots in a square formation, with the flying camera undergoing a circular motion. The results from it are displayed in Fig. 5. We show the performance of the homography-based control with and without collision avoidance. In both cases the multi-robot system reaches the desired configuration (i.e. the relative positions between the robots in the formation). It can be seen that the collision avoidance mechanism performs well and generates more suitable paths from a practical point of view. As explained in section III-B, the control is performed in one single step and the final orientation of the robots is not corrected. The evolution of the homography entries is also displayed in the figure. As can be seen, all the individual homographies computed between each pair of robots converge to the desired homography. Notice that the desired homography is not constant, as it evolves depending on the motion of the camera.

In the second experiment, the desired configuration is a triangle formed by six robots, while the flying camera follows a spiral-like motion. Figure 6 displays the results from this experiment. Again, the target multi-robot configuration is correctly achieved, independently of the motion of the camera or the absolute position of the robot team. The minimum distance between robots is shown in order to illustrate the collision avoidance performance. Finally, we also carried out an experiment with a larger number of robots (twenty). It can be seen in Fig. 6 that in this case, the minimum distance between robots is also maintained above a certain threshold, avoiding drops in its value (possible collisions).

V. Conclusion

A new visual control scheme has been proposed to lead a group of robots to a desired configuration. The control law is based on a particular homography parametrization that allows to define the desired location of the robots in the image plane. The advantages of this approach are the simplicity of the definition of any arbitrary desired configuration for the set of robots, avoiding the need of metric information in the 3D space, and the fact that the planar motion of the flying camera can be unknown and arbitrary (thus allowing it to perform additional tasks simultaneously) without affecting the control performance. A vision-based collision avoidance method decoupled from the control task is also proposed. Simulations are presented in order to support the validity of the approach and illustrate its performance.

References

[1] A. K. Das, R. Fierro, V. Kumar, J. P. Ostrowski, J. Spletzer, and C. J. Taylor, "A vision-based formation control framework," *IEEE Transactions on Robotics and Automation*, vol. 18, pp. 813–825, 2002.

[2] R. Vidal, O. Shakernia, and S. Sastry, "Following the flock: Distributed formation control with omnidirectional vision-based motion segmentation and visual servoing," *Robotics and Automation Magazine*, vol. 11, no. 4, pp. 14–20, 2004.

[3] J. Chen, D. Sun, J. Yang, and H. Chen, "Leader-Follower Formation Control of Multiple Non-holonomic Mobile Robots Incorporating a Receding-horizon Scheme," *The International Journal of Robotics Research*, vol. 29, no. 6, pp. 727–747, 2010.

[4] F. Chaumette and S. Hutchinson, "Visual servo control, part I: Basic approaches," *IEEE Robotics and Automation Magazine*, vol. 13, no. 4, pp. 82–90, Dec. 2006.

[5] H. Chen, D. Sun, and J. Yang, "Global localization of multirobot formations using ceiling vision SLAM strategy," *Mechatronics*, vol. 19, no. 5, pp. 617 – 628, 2009.

[6] G. López-Nicolás, J. J. Guerrero, and C. Sagüés, "Visual control of vehicles using two-view geometry," *Mechatronics*, vol. 20, no. 2, pp. 315 – 325, 2010.

[7] G. Blanc, Y. Mezouar, and P. Martinet, "Indoor navigation of a wheeled mobile robot along visual routes," in *IEEE International Conference on Robotics and Automation*, April 2005, pp. 3365–3370.

[8] J. Courbon, Y. Mezouar, and P. Martinet, "Indoor navigation of a non-holonomic mobile robot using a visual memory," *Autonomous Robots*, vol. 25, no. 3, pp. 253–266, 2008.

[9] G. López-Nicolás, N. R. Gans, S. Bhattacharya, J. J. Guerrero, C. Sagüés, and S. Hutchinson, "Homography-based control scheme for mobile robots with nonholonomic and field-of-view constraints," *IEEE Transactions on Systems, Man, and Cybernetics, Part B*, vol. 40, no. 4, pp. 1115–1127, 2010.

[10] O. Khatib, "Real-time obstacle avoidance for manipulators and mobile robots," *Int. Journal of Robotics Research*, vol. 5, pp. 90–98, 1986.

[11] Y. Koren and J. Borenstein, "Potential field methods and their inherent limitations for mobile robot navigation," in *IEEE International Conference on Robotics and Automation*, 1991, pp. 1398–1404.

[12] S. S. Ge and Y. J. Cui, "Dynamic motion planning for mobile robots using potential field method," *Autonomous Robots*, vol. 13, pp. 207–222, 2002.

[13] W. H. Huang, B. R. Fajen, J. R. Fink, and W. H. Warren, "Visual navigation and obstacle avoidance using a steering potential function," *Robotics and Autonomous Systems*, vol. 54, no. 4, pp. 288 – 299, 2006.

[14] D. E. Chang, S. C. Shadden, J. E. Marsden, and R. Olfati-Saber, "Collision avoidance for multiple agent systems," *IEEE International Conference on Decision and Control*, pp. 539–543, 2003.

[15] N. Moshtagh, N. Michael, A. Jadbabaie, and K. Daniilidis, "Vision-based, distributed control laws for motion coordination of nonholonomic robots," *IEEE Transactions on Robotics*, vol. 25, no. 4, pp. 851–860, 2009.

[16] G. López-Nicolás, Y. Mezouar, and C. Sagüés, "Homography-based multi-robot control with a flying camera," in *IEEE International Conference on Robotics and Automation*, 2011, pp. 4492–4497.

[17] R. I. Hartley and A. Zisserman, *Multiple View Geometry in Computer Vision*, 2nd ed. Cambridge University Press, 2004.

[18] E. Rimon and D. Koditschek, "Exact robot navigation using artificial potential fields," *IEEE Transactions on Robotics and Automation*, vol. 8, no. 5, pp. 501–518, 1992.

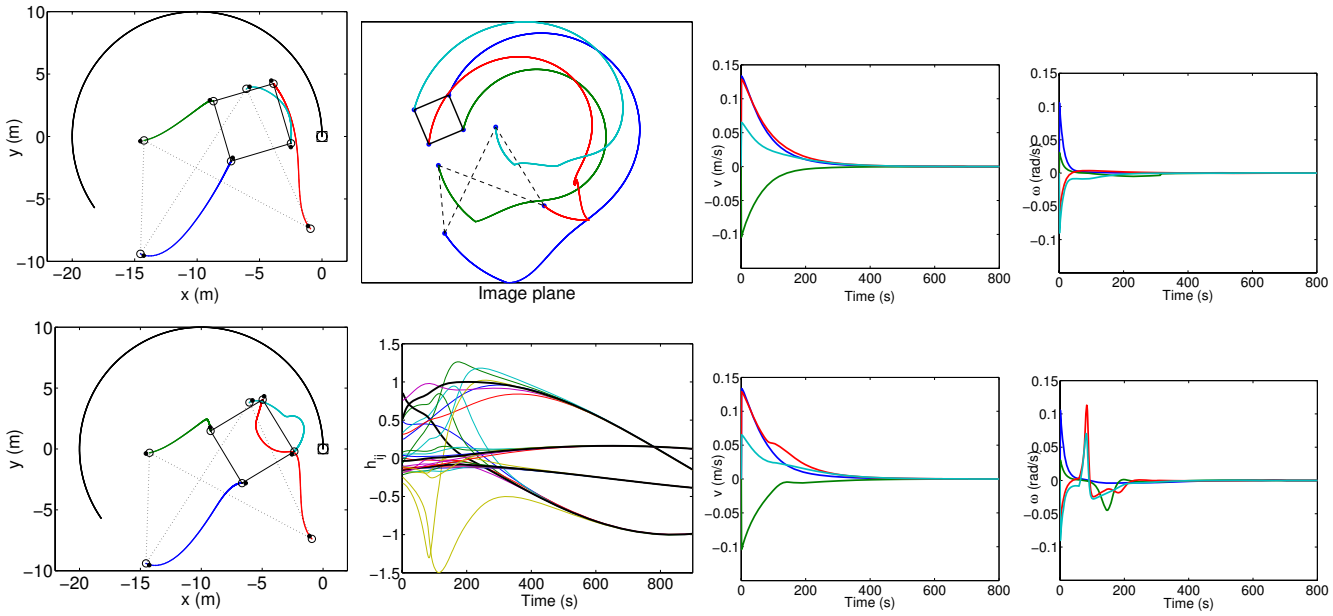

Fig. 5. Simulation with the flying camera undergoing a circular motion. The robots are initially in an arbitrary configuration and the goal is to reach the desired one, which is defined by the image of a square with vertices of $x-y$ coordinates: (-10,-8),(-10,-3),(-5,-8),(-5,-3). Top-left: top view of the camera (the initial position is depicted with a circle inside a square) and the robots, which are depicted as circles with a spot signalling their orientation. The initial configuration is drawn with a dashed line and the path followed by the robots to reach the desired configuration is shown (thick lines). This plot corresponds to the case where collision avoidance is not used. Top row-second column: trace of the robots in the image plane. Top row-third and fourth columns: linear and angular velocities of the robots, without collision avoidance. Bottom-left: robot paths with collision avoidance. Bottom row-second column: evolution of the homography entries (h_{11}, h_{12}, h_{13}, h_{23}) of the desired homography (thick lines) and the current homographies between the robots (thin lines). Bottom row-third and fourth columns: linear and angular velocities of the robots, with collision avoidance. The image plane and homography elements plots are from the case when collision avoidance is used.

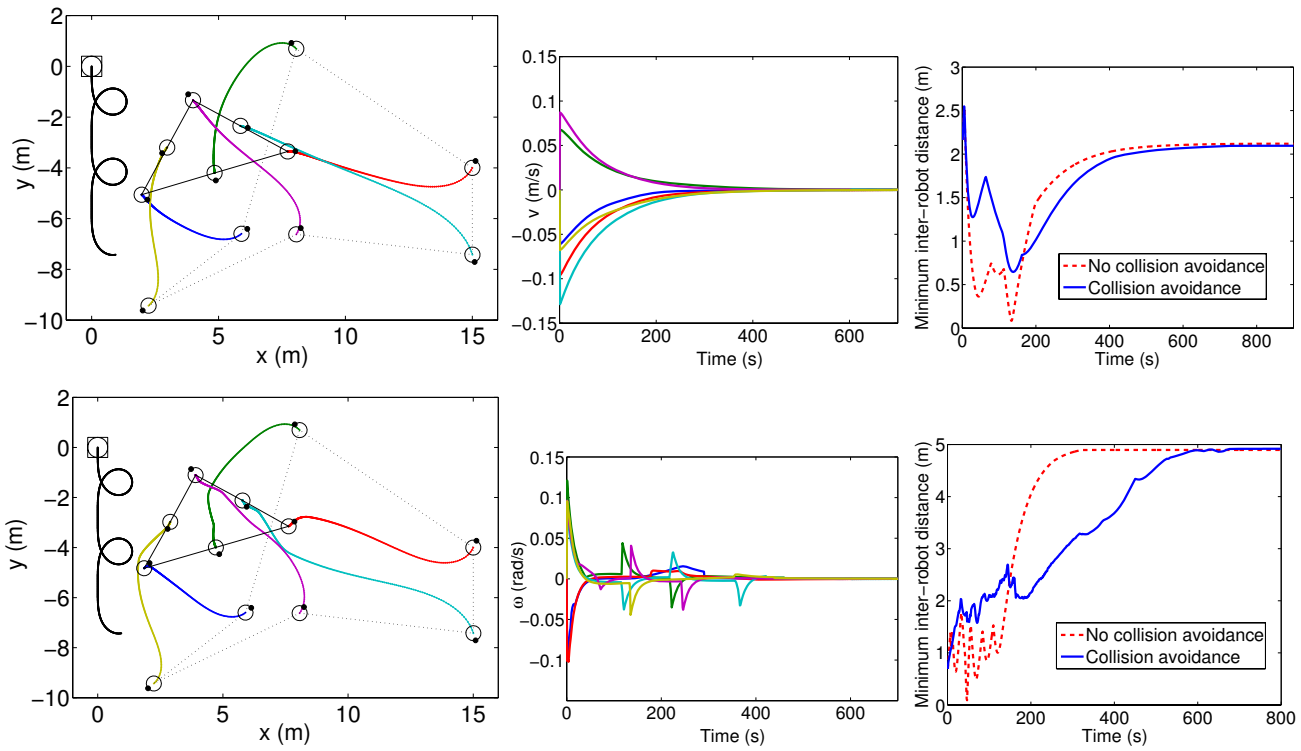

Fig. 6. Simulation results with the flying camera undergoing a spiral-like motion. The robots are initially in an arbitrary configuration and the goal is to reach the desired one, which is a triangle formed by six robots. Top-left: camera motion and robot paths, without collision avoidance. Bottom-left: camera motion and robot paths, with collision avoidance. Top row-center: linear velocities. Bottom row-center: angular velocities. The displayed velocities are for the case in which collision avoidance is used. Top-right: minimum inter-robot distance, with and without collision avoidance, for the six-robot triangular configuration. Bottom-right: minimum inter-robot distance, with and without collision avoidance, for a twenty-robot square configuration with circular camera motion.